# PI3K pathway regulates survival of cancer stem cells residing in the perivascular niche following radiation in medulloblastoma in vivo

Dolores Hambardzumyan,[1,2] Oren J. Becher,[1,2,3] Marc K. Rosenblum,[2,4] Pier Paolo Pandolfi,[5,6] Katia Manova-Todorova,[7] and Eric C. Holland[1,2,8,9]

[1]Department of Cancer Biology and Genetics, Memorial Sloan-Kettering Cancer Center, New York, New York 10021, USA; [2]Brain Tumor Center, Memorial Sloan-Kettering Cancer Center, New York, New York 10021, USA; [3]Department of Pediatrics, Memorial Sloan-Kettering Cancer Center, New York, New York 10021, USA; [4]Department of Pathology, Memorial Sloan-Kettering Cancer Center, New York, New York 10021, USA; [5]Cancer Genetics Program, Beth Israel Deaconess Cancer Center, Harvard Medical School, Boston, Massachusetts 02215, USA; [6]Department of Medicine, Beth Israel Deaconess Medical Center, Harvard Medical School, Boston, Massachusetts 02215, USA; [7]Molecular Cytology Core Facility, Memorial Sloan-Kettering Cancer Center, New York, New York 10021, USA; [8]Department of Surgery (Neurosurgery), Memorial Sloan-Kettering Cancer Center, New York, New York 10021, USA

**Medulloblastomas are brain tumors that arise in the cerebellum of children and contain stem cells in a perivascular niche thought to give rise to recurrence following radiation. We used several mouse models of medulloblastomas in parallel to better understand how the critical cell types in these tumors respond to therapy. In our models, the proliferating cells in the tumor bulk undergo radiation-induced, p53-dependent apoptotic cell death. Activation of Akt signaling via PTEN loss transforms these cells to a nonproliferating extensive nodularity morphology. By contrast, the nestin-expressing perivascular stem cells survive radiation, activate PI3K/Akt pathway, undergo p53-dependent cell cycle arrest, and re-enter the cell cycle at 72 h. Furthermore, the ability of these cells to induce p53 is dependent on the presence of PTEN. These cellular characteristics are similar to human medulloblastomas. Finally, inhibition of Akt signaling sensitizes cells in the perivascular region to radiation-induced apoptosis.**

Previous studies have shown the existence of a small subpopulation of cells in brain tumors that share key characteristics with neuronal stem/progenitor cells. These findings suggest that brain tumors contain "cancer stem cells" that may be critical for tumorigenesis (Ignatova et al. 2002; Hemmati et al. 2003; Singh et al. 2003). Brain tumor stem cells positive for nestin and CD133 occupy a perivascular niche (PVN) and a disruption of that microenvironment ablates the self-renewing cell population in brain tumors and arrests tumor growth (Calabrese et al. 2007). Nestin has been shown to be a strong prognostic factor for glioma malignancy (Strojnik et al. 2007). Furthermore, brain tumor cells expressing the stem cell marker CD133 have been shown to be relatively resistant to radiation by preferential activation of the DNA damage response (Bao et al. 2006). However, the molecular pathways governing such stem-like behavior remain largely elusive.

Many critical questions surrounding the biology of therapeutic response in tumor stem-like cells remain to be answered. For example, are the stem-like cells in the niche the ones resistant to therapy, and does the niche provide additional protection for the stem-like cells that is independent of the DNA damage response? Does the relatively low cycling of stem-like cells contribute to their resistant character, or does radiation cause cell cycle arrest in the stem-like cells that are cycling at the time of treatment? Furthermore, what is the time interval between radiation treatment and the point when the stem-like cells re-enter the cell cycle? Do the mutations commonly found in some types of brain tumors, such as p53 or PTEN loss, affect the therapeutic response of either the resistant stem-like cells or the non-stem-like cell populations? Finally, are there signaling pathways that contribute to the resistance phenotype in these cells? All of these questions are crucial because there are small-molecule inhibitors of signaling pathways already available that in theory could reduce the radiation resistance specifically of the stem-like cell population in vivo (Hambardzumyan et al. 2006). In order to address some

of these questions we used medulloblastomas because of their relative radiation sensitivity that results in a less complex cellular response than what is found in gliomas.

Medulloblastomas are the most common primary CNS tumors in children, comprising ~20% of all pediatric primary CNS tumors (Packer 1990). Standard therapy for medulloblastoma patients includes surgery and irradiation followed by chemotherapy, leading to 50%–80% 5-yr survival. These tumors are radiosensitive; however, long-term side effects of radiation therapy have led to attempts to decrease the amount of craniospinal and local tumor site irradiation, with resultant disease relapse (Landberg et al. 1980; Hershatter et al. 1986; Deutsch et al. 1996). The doses of radiation delivered at the primary site and neuroaxis in children with medulloblastoma have been chosen empirically and not optimized by randomized studies.

Although many medulloblastoma cell lines and xenograft models have been developed, genetic alterations, microenvironment, anatomical location, and developmental time frame of these tumors differ from human tumors in their in vivo setting. All of these parameters affect the tumor's response to therapy. Gene expression profiles of medulloblastomas have provided helpful information for successful mouse modeling of this tumor (Pomeroy et al. 2002; Lee et al. 2003). The human *Ptc* gene is a tumor suppressor and developmental regulator (Hahn et al. 1996). *Ptc* gene mutations occur in 3%–14% of human sporadic medulloblastomas (Pietsch et al. 1997; Raffel et al. 1997; Wolter et al. 1997). Ptc is a key component of Hedgehog (Hh) signaling pathway, which is a major regulator of cerebellar development where Sonic Hedgehog (SHH) secreted by the Purkinje cells promotes the proliferation of cells in the external granule layer (EGL) (Hammerschmidt et al. 1997; Dahmane and Ruiz i Altaba 1999; Wallace 1999; Wechsler-Reya and Scott 1999). In mice, heterozygous mutation of *Patched-1* (*Ptc1*) is associated with an ~20% incidence of medulloblastoma over a period of 1 yr (Goodrich et al. 1997; Wetmore et al. 2000; Corcoran and Scott 2001). $Ptc^{+/-}$ mice are hypersensitive to ionizing radiation, and DNA damage induced by radiation in these mice induces medulloblastoma in an age-dependent manner, ranging from 81% in the cerebellum irradiated at postnatal day 1 (P1) to 3% in the cerebellum irradiated at P10 (Pazzaglia et al. 2006).

In mice, p53 dysfunction in conjunction with deletions in genes controlling the cell cycle, apoptosis, and DNA repair, such as *Ptc*, *Rb*, DNA ligase IV, *PARP-1*, *Kip1*, *Ink4d*, and *Ink4c* leads to the formation of tumors having histology consistent with medulloblastoma (Marino et al. 2000; Wetmore et al. 2001; Lee and McKinnon 2002; Pazzaglia et al. 2002; Tong et al. 2003; Zindy et al. 2003). However, p53 is wild type in 92%–99% of human sporadic medulloblastomas (Cogen and McDonald 1996; Portwine et al. 2001) and p53 status is clearly linked to radiation responses in several other tumor types (Schmitt et al. 2002). It has been suggested that increased p53 staining (implying p53 dysfunction) is associated with a poor prognosis, and is more common in anaplastic medulloblastoma, known to have a worse clinical outcome, and p53 inactivation is associated with decreased levels of radiation-induced apoptosis in medulloblastoma cell lines (Dee et al. 1995; Woodburn et al. 2001; Eberhart et al. 2005). Therefore, preclinical trials that include radiation therapy using p53-deficient models of medulloblastoma may generate results inconsistent with the majority of these tumors in humans. However, there are several p53 wild-type models of medulloblastoma that are more accurate in this regard.

Somatic cell gene transfer with retroviral vectors has been used to model medulloblastoma. MLV-based retroviral transfer of SHH to the cerebellum of p53 wild-type mice in utero generated medulloblastomas (Weiner et al. 2002). In addition, the RCAS/tv-a system, which allows postnatal gene transfer in a cell-type-specific manner (Holland and Varmus 1998; Fisher et al. 1999), has been used to generate medulloblastomas by targeting the expression of SHH and c-Myc to p53 wild-type nestin-expressing neural stem cells (Rao et al. 2003). Infection with RCAS-SHH alone generated medulloblastomas at a low frequency, which was increased substantially by concurrent infection with RCAS-Akt, RCAS-IGF2 or RCAS-N-myc (Rao et al. 2004; Browd et al. 2006).

In the present study, we investigated the mechanism of radiation response in medulloblastomas and determined whether regional cellular radioresistance in these tumors is associated with stem cells. We used several mouse modeling systems for medulloblastoma including those based on *Ptc* heterozygosity, as well as somatic cell gene transfer with the RCAS/tv-a system to transfer SHH in conjunction with Akt or N-myc to nestin-expressing cells. Following γ-ionizing irradiation (γIR), at least three different populations of tumor cells were observed. The main cell population, the tumor bulk (TB), underwent p53-dependent apoptotic cell death. The two other populations were resistant to radiation: nestin-expressing stem cells in the PVN that underwent a p53-dependent cell cycle arrest, and a nonproliferating cell population of neuronal differentiation in regions of extensive nodularity (EN) that showed no response to radiation. We demonstrate that radiation activates the Akt/mTOR pathway in the perivascular nestin-expressing stem cells, that these cells re-enter the cell cycle at 72 h, and that these cells are responsible for the tumor recurrence. We also developed a novel medulloblastoma model using the RCAS/tv-a methodology by SHH overexpression and PTEN loss that corresponds to a histological variant of human medulloblastoma called medulloblastoma with EN. Using this model, we show that the p53-dependent cell cycle arrest of nestin-expressing perivascular cells is also PTEN-dependent, and that Akt activation correlates with nestin expression in the PVN. Lastly, we show that the loss of PTEN in the TB drives cell differentiation toward a neuronal lineage. We demonstrated that inhibition of radiation-induced Akt phosphorylation sensitizes PVN to radiation-induced apoptosis.

## Results

### Medulloblastoma models contain three distinct cell types

Because of the known effect of p53 on therapeutic responses in other tumor types we specifically chose to study p53 wild-type models. It was shown by the Fults group (Browd et al. 2006) that tumors induced by the RCAS/tv-a methodology are mixtures of clones originating from cells infected with SHH alone or in combination with N-myc or Akt, and there is variation from tumor to tumor. To ensure that our observations were not model-specific or due to single or combined viral distribution in the cells, we compared the data from several different medulloblastoma models. More specifically, we were interested in the biology of the largest subset of medulloblastomas including $Ptc^{+/-}$ mice irradiated at P1 (Pazzaglia et al. 2006), spontaneous $Ptc^{+/-}$ tumors (Goodrich et al. 1997; Wetmore et al. 2000; Corcoran and Scott 2001), and RCAS/tv-a based somatic cell gene transfer models with combined overexpression of SHH + Akt or SHH + N-myc (Browd et al. 2006). Although the incidence of medulloblastomas in these models varies, the general histology of these tumors is quite similar, and all are p53 wild type.

We initially characterized these models focusing specifically on the cells adjacent to the blood vessels in the PVN. These cells were distinct from cells comprising the bulk of the tumor; they exhibited a variable but substantial proliferation rate detected by proliferating cell nuclear antigen (PCNA) and phospho-Histone H3 (pH3), and were characterized by low levels of expression of the cytoskeletal protein nestin, a marker of neuronal stem and progenitor cells (Supplemental Fig. 1A,C; Yuan et al. 2004).

The non-PVN area or TB was comprised of two cell populations. The major one contained cells that were highly proliferative, bmi1-expressing, NeuN-negative cells with desmoplastic or classic medulloblastoma histological features (Supplemental Fig. 1A,B). A smaller subpopulation of the TB (accounting for 20% of the tumor mass, in only ~20% of tumors) was composed of cells with a very low proliferation rate and a higher level of pAkt expression (data not shown). These cells also expressed high levels of neuronal marker NeuN, resembling a subset of human medulloblastomas called medulloblastomas with EN (Supplemental Fig. 1A,D). These three cell types (the PVN cells and the two types of TB cells) were seen in all models (SHH alone, $n = 5$; SHH + Akt, $n = 5$; SHH + N-myc, $n = 5$).

### Radiation induces apoptosis specifically in proliferating cells of the TB

Next, we determined the response of the three cell types to 2 Gy of γIR, the equivalent of a single fraction used for these tumors in patients. At 6 h post-radiation, 80% of the cells underwent apoptosis as indicated by morphology and cleaved caspase-3 immunodetection (SHH + N-

myc, $n = 2$; SHH + Akt, $n = 2$) (Fig. 1A,B). The dying cells were limited to the TB. There was a complete overlap of cleaved caspase-3 expression with expression of PCNA (Fig. 1C,D), indicating that essentially all dividing cells in the TB were undergoing cell death within 6 h following a single dose of radiation. Similar results were obtained after irradiating spontaneous tumors in $Ptc^{+/-}$ mice with 2 Gy and tumors in the $Ptc^{+/-}$ mice that were irradiated with 3 Gy γIR at P1 ($n = 6$) (Supplemental Fig. 2A–C).

### Cells of the PVN are arrested within 6 h of irradiation and re-enter the cell cycle in 72 h

Cells in the PVN and a subset of cells in the TB survived irradiation. The first group of surviving cells was contained EN cells of the TB (by H&E; PCNA not shown) with a very low proliferating rate prior to irradiation (Fig. 2A). The second group consisted of the cells of the PVN, most of which were proliferating prior to irradiation (Fig. 2B,C) and showed elevated nestin expression levels at 6 h post-2-Gy γIR (Fig. 2D). It has been shown that GFAP and nestin double-positive B cells in SVZ are the stem cells in the normal brain (Alvarez-Buylla et al. 2002); therefore, we performed GFAP staining in PVN, GFAP-positive cells are a subset of nestin-positive surviving PVN cells (Supplemental Fig. 3). To further characterize nestin-positive surviving PVN cells we stained them with progenitor marker Olig2. Olig2-positive cells are a subset of nestin-positive surviving PVN as well (Supplemental Fig. 4), although there is a small subset of Olig2-positive and nestin-negative cells that undergo apoptosis post-2-Gy radiation (data not shown). We studied the fate of these arrested nestin-positive PVN cells over time by irradiating SHH + Akt and SHH + N-myc tumor-bearing mice with 2 Gy γIR and sacrificing them at different time points following treatment (untreated, $n = 5$; 4 h, $n = 2$; 6 h, $n = 4$; 8 h, $n = 2$; 12 h, $n = 2$; 24 h, $n = 2$; 48 h, $n = 3$; 72 h, $n = 3$) (Fig. 3A). The tumors were examined for proliferation and apoptosis. Consistent with the above data, we found that cleaved caspase-3 and terminal deoxynucleotidyltransferase-mediated dUTP-biotin nick end-labeling (TUNEL) staining were induced by 6 h after irradiation, and that proliferation as measured by PCNA was reduced in the surviving cells. By 12 h, there was no evidence of proliferation within the tumors. At 48 h post-irradiation, a very small number of cells began to re-enter the cell cycle, and at 72 h there were clusters of cells staining for the proliferation markers PCNA and phospho-histone H3. Further analysis of tumors harvested at 72 h indicated that these clusters of cycling cells were perivascular nestin-expressing cells (Fig. 3B; Supplemental Fig. 5).

### PVN cells surviving irradiation show substantial activition of the Akt/mTOR pathway

Because of the connection between Akt activity and cell survival (Ahmed et al. 1997; Kennedy et al. 1997; Kulik
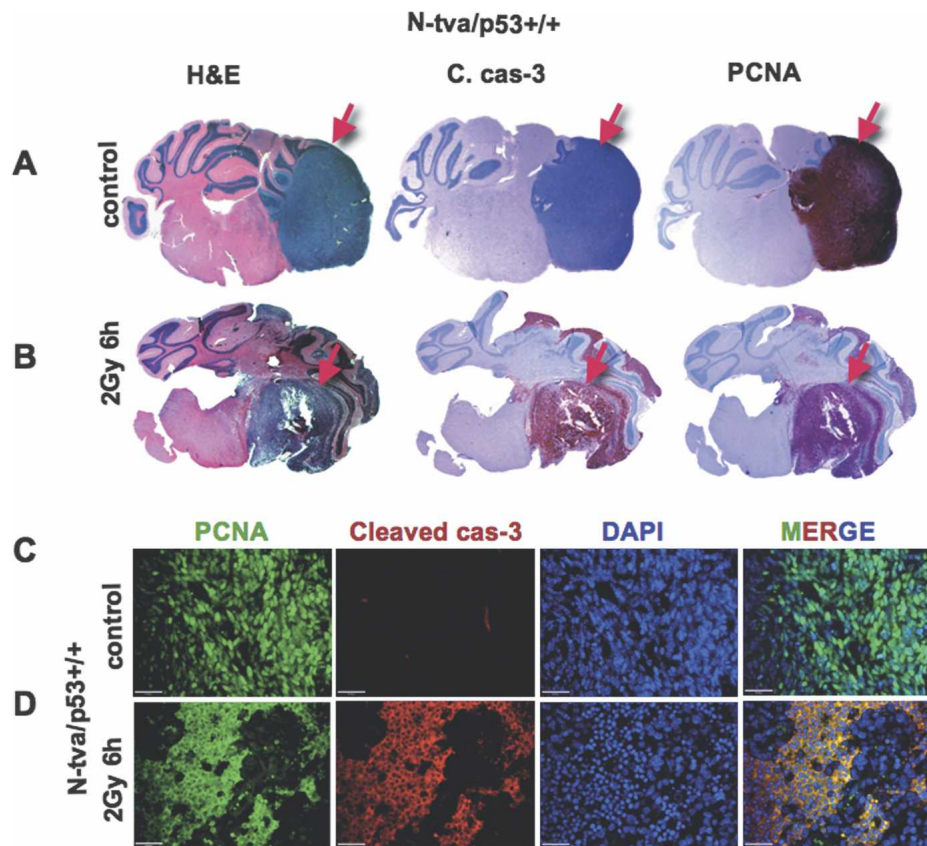
**Figure 1.** Radiation induces apoptosis in TB of medulloblastoma. (*A*) Whole mount of control nonirradiated medulloblastoma (SHH + N-myc representative pictures). (*B*) Whole mount of 6-h-post-2-Gy γIR, stained for H&E, cleaved caspase-3 indicating apoptosis, and PCNA indicating proliferation (red arrows indicate tumors). Immunofluorescence detection of PCNA (green), cleaved caspase-3 (red), and DAPI (blue) of untreated (*C*) and irradiated (*D*) tumors (SHH + N-myc, $n = 2$; SHH + Akt, $n = 2$). As a result of irradiation, PCNA is excluded from the nuclei and colocalizes with cleaved caspase-3 in the cytoplasm of the TB cells (yellow color on the merged image) Bars: *C,D*, 20 µm.

et al. 1997; Songyang et al. 1997), and between pS6RP activity and proliferation in the developing cerebellum, we characterized the activity of the components of the PI3K pathway in the different cell types of our tumor models. We investigated the Akt pathway by immunohistochemistry in the nonirradiated tumors induced by the combination of SHH + N-myc and SHH + Akt overexpression. Both tumor types showed high PTEN levels. The SHH + Akt tumors showed a low diffuse pAkt S473 staining (Supplemental Fig. 6A); the pAkt staining in the SHH + N-myc tumors was almost undetectable (data not shown).

In response to irradiation, PTEN staining was lost in the dying cells of the TB. The PVN cells showed detectable PTEN, and increased pAkt staining. Radiation-induced activation of the Akt pathway in the PVN reached the maximum effect at 6 h (Supplemental Fig. 6B) and correlated with a peak in nestin and pS6RP expression in the same cells at the same time (Fig. 4A). Nestin and pS6RP immunoreactivity was 2.9 and 2.3 times higher, in the SHH + Akt and SHH + N-myc medulloblastomas, respectively, at 6 h following irradiation as compared with controls (Fig. 4B,C). The elevation of pAkt and

pS6RP levels was accompanied by a slight decrease in PTEN expression in the PVN (Supplemental Fig. 6B). Therefore, the surviving cells had either high baseline Akt pathway activity prior to irradiation (in the case of the EN cells) (data not shown) or low Akt activity that was increased by irradiation, concurrent with cell cycle arrest (as in the case of the cells of the PVN). In order to verify that we were not investigating a mouse-specific phenomenon, we stained human frozen medulloblastoma specimens and found the existence of stem cell niches with expression of nestin, notch receptor (shown to be important for maintenance of neuronal stem cells) (Hitoshi et al. 2002) and pS6RP in the perivascular regions surrounding CD31^{+} vascular structures in these tumors ($n = 15$) (Fig. 4D). In the mouse tumors, we also noted small regions of nonproliferating cells, high NeuN-expressing regions that had low detectable PTEN levels, and higher pAkt and pS6RP staining (data not shown). These regions correspond to medulloblastoma with EN in humans and, therefore, are referred to as EN. The characteristics of this cell type were not significantly changed by radiation (Supplemental Fig. 7A–D).
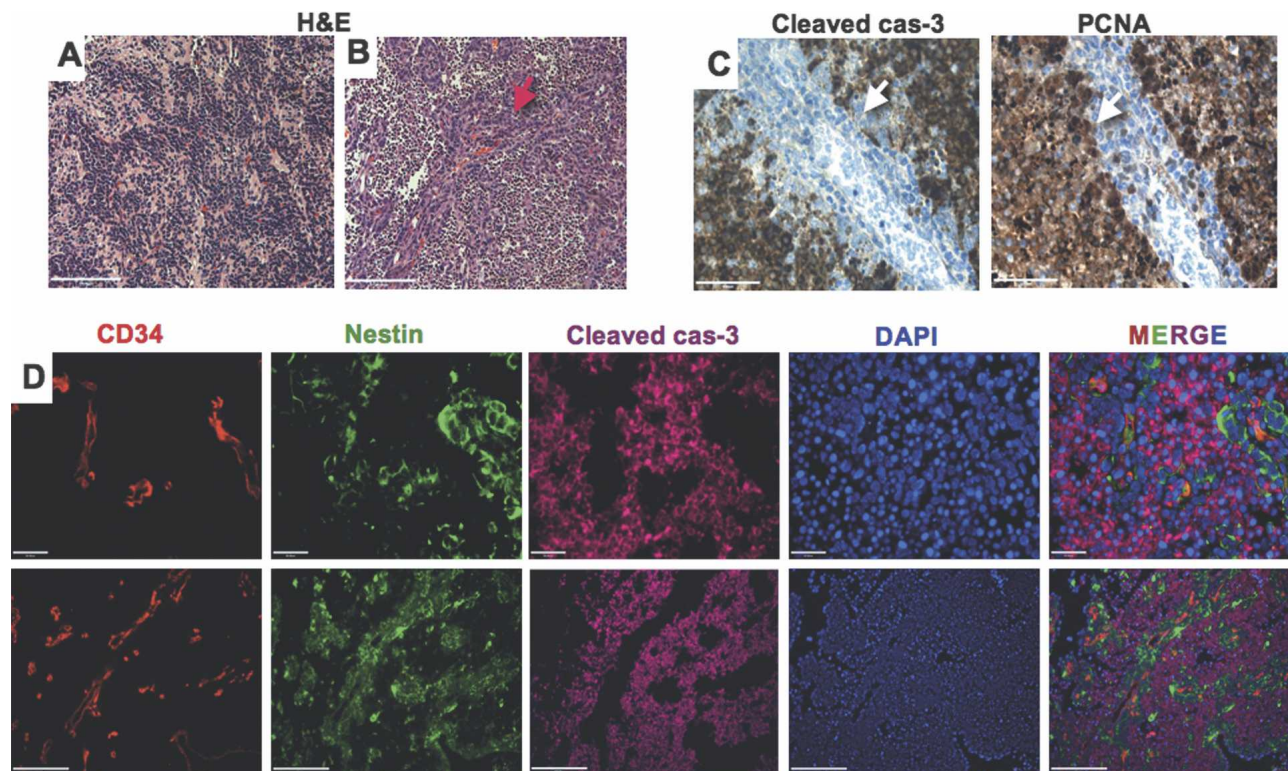
**Figure 2.** Two distinct medulloblastoma cell populations survive 2 Gy of γIR. H&E staining for cells of the EN (*A*) and cells of the PVN (*B*) (red arrow) (SHH + N-myc representative pictures). (*C*) Cleaved caspase-3 and PCNA staining showing lack of cleaved caspase-3 and proliferation in the surviving cells of the PVN. Surviving PVN cells are adjacent to blood vessels, express nestin, and are cleaved caspase-3-negative (white arrows). (*D*) High- and low-magnification images of triple immunostaining with CD34 (red), nestin (green), cleaved caspase-3 (magenta), and DAPI counterstaining (blue) show that all surviving PVN cells are nestin-positive. Bars: *A*–*C*, 50 μm; *D*, 20 and 100 μm.

*Loss of PTEN in combination with SHH overexpression leads to EN histology formation in TB and proliferation in the PVN*

The various models of medulloblastoma we used demonstrated activation of the Akt pathway in response to radiation when the *PTEN* gene was wild type. In order to determine the role of PTEN specifically in these tumors, we created a model of medulloblastoma with PTEN loss using Ntv-a mice with floxed *PTEN* and infected them with RCAS-SHH + RCAS-Cre. The majority of the tumors that arose showed nearly 100% EN in the TB (meaning that all TB was composed of the EN) in most of the cases (70% of tumors); in 30% of tumors we noticed some highly proliferating regions that were *PTEN*-positive and represented ~10%–30% of the tumor area. The tumors were stained for PTEN expression, pAkt S473, and pAkt T308 in order to verify that the PTEN gene was deleted (n = 5) (Fig. 5A,B; Supplemental Fig. 8A). This result was consistent with EN regions of medulloblastomas with wild-type PTEN where we noted low PTEN and high pAkt levels, suggesting that Akt activation drives EN histology (data not shown). Consistent with NeuN expression in the EN regions with low PTEN in wild-type PTEN medulloblastomas, the PTEN-deficient tumors had very high levels of NeuN. The only

cells that were NeuN-negative were in the PVN (Fig. 5C,D).

The PVN of PTEN-deficient tumors was highly proliferative; in fact, it was the only proliferative region in the tumors because the EN cells that comprised the bulk of these tumors showed essentially no proliferation (Fig. 5A,B). Further characterization of the PVN in these PTEN-deficient tumors (n = 5) showed high levels of pAkt and pS6RP staining consistent with the loss of PTEN, and they were the only cells that showed elevated nestin expression and were proliferating (Fig. 5C,D; Supplemental Fig. 8A,B). The elevated pAkt/pS6RP and nestin expression levels were similar to those seen in the PVN of PTEN wild-type tumors at 6 h post-2-Gy γIR. The difference was that in the wild-type tumors the cells of the PVN arrested following irradiation, while the PVN cells in the PTEN-deficient tumors were highly proliferative and arrest did not occur. The nonproliferating EN showed no effect after irradiation; this was consistent with the EN regions of the wild-type tumors that had low PTEN expression and showed no response to radiation (n = 2 each at 6 and 24 h post-2-Gy γIR) (data not shown).

These data indicate that the cell cycle arrest seen in the PVN of wild-type medulloblastomas is PTEN-dependent.
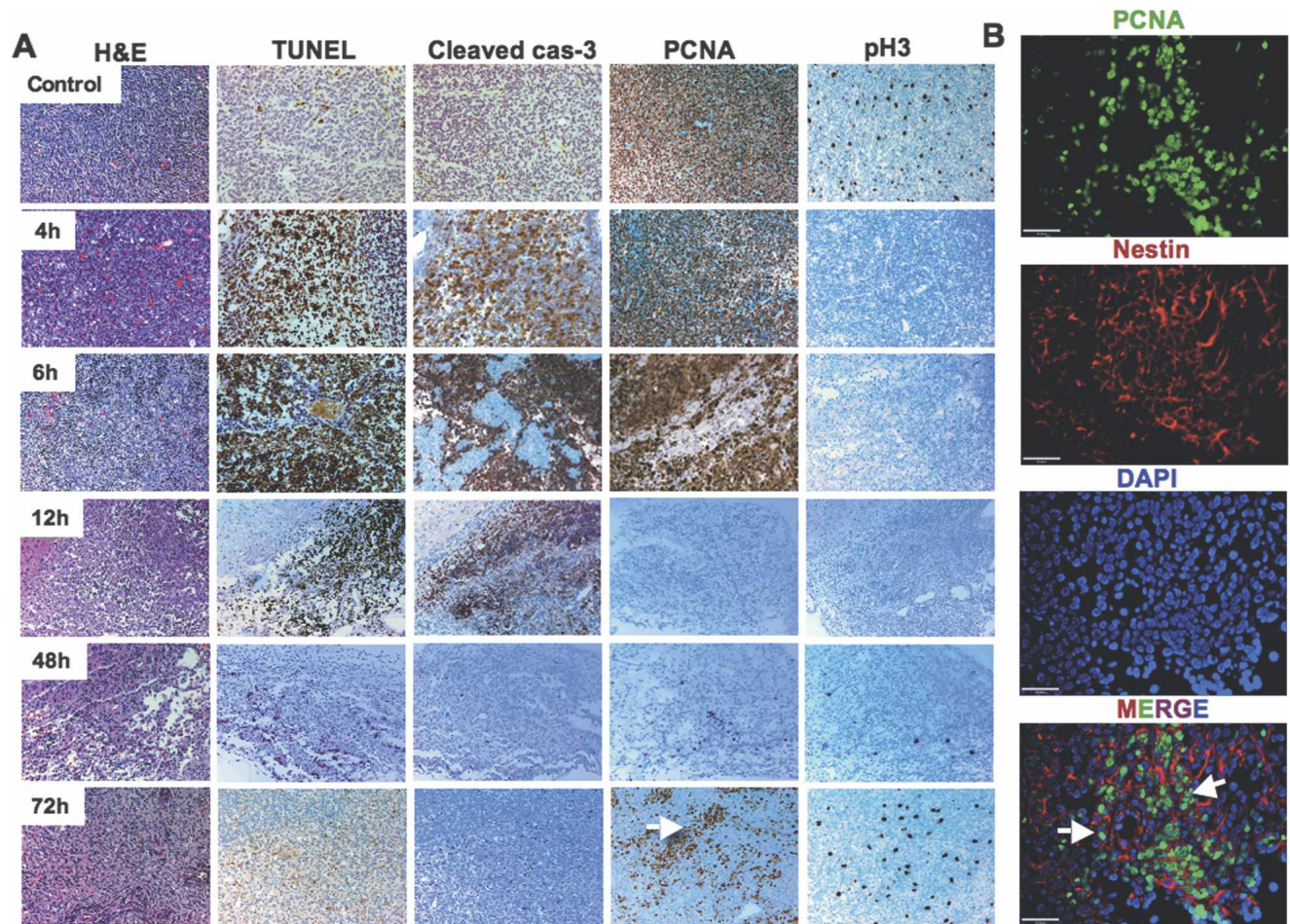
**Figure 3.** Evaluation of cell death and proliferation over time following 2 Gy of γIR in p53$^{+/+}$ medulloblastomas. Cells surviving 2 Gy of γIR in the PVN re-enter the cell cycle at 72 h. (*A*) H&E, TUNEL, cleaved caspase-3, PCNA, and pH3 of untreated tumors and tumors treated by 2 Gy of γIR were collected after 4, 6, 12, 48, and 72 h, as indicated. Clusters of cells re-enter the cell cycle at 72 h (white arrow). (*B*) Triple immunofluorescent staining of PCNA (green), nestin (red), and DAPI (blue) at 72 h after 2 Gy of γIR in PVN shows high proliferation of nestin-positive cells (white arrows). Bars: *A*, 100 μm; *B*, 20 μm.

## *p53 protein levels are induced in two distinct waves following irradiation*

p53 is involved in both radiation-induced cell cycle arrest and apoptosis, and its connections to PTEN are well-documented in other cell types (Yan et al. 2006). Therefore, we investigated the radiation-induced elevation of the total p53 protein in our SHH + Akt and SHH + N-myc medulloblastoma models (Ntv-a p53 wild-type, *n* = 4 at 4 and 6 h following γIR). In the nonirradiated tumors, there were few p53-positive cells. However, following irradiation there was an increase in total p53 levels that occurred in two cell types in two distinct time courses (Fig. 6A). The proliferating TB undergoing apoptosis in response to radiation showed elevated p53 staining that peaked at 4 h. At this time point, these cells were already in the process of dying and the staining for p53 was mainly cytoplasmic (as was PCNA). The cells of the PVN did not stain for p53 at 4 h. By 6 h, the nuclei of the apoptotic cells became pyknotic and no longer showed detectable p53 staining. Additionally, while p53

staining was lost in the apoptotic cells, the cells of the PVN now showed strong nuclear p53 staining (Fig. 6A). This second wave of p53 staining was concurrent with cell cycle arrest, elevation of Akt activity, and the elevation of nestin expression described for these PVN cells.

## *Radiation-induced elevation of p53 is PTEN-dependent*

We performed immunohistochemical staining for p53 on the PTEN-deficient medulloblastomas before (*n* = 5) and 6 h after irradiation (*n* = 2). The PTEN-deficient EN showed no p53 staining before or after radiation (data not shown). This was consistent with the fact that the EN regions in wild-type tumors showed low PTEN staining and no elevation of p53 protein in response to radiation (Fig. 6A). Cells in the PVN that were highly proliferative in the PTEN-deficient nonirradiated tumors did not show cell cycle arrest, nor did they elevate p53 levels following irradiation. These data indicate that radiation-
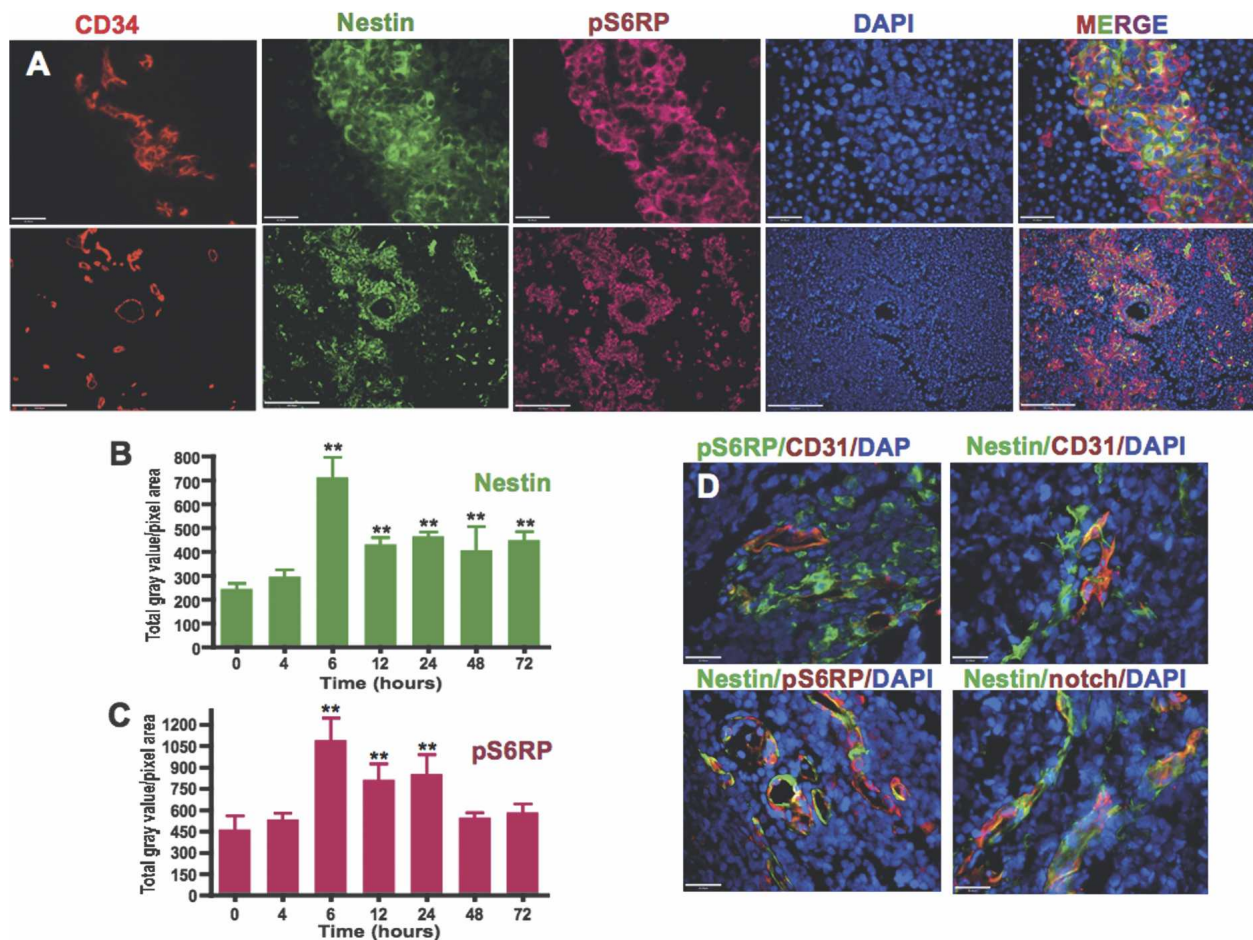
**Figure 4.** Radiation induces elevation of nestin and pS6RP expression in the cells of the PVN. (*A*) High and low magnification of triple immunofluorescent staining of CD34 (red), nestin (green), pS6RP (magenta), and DAPI (blue) following 6 h of 2 Gy of γIR (SHH + N-myc). Quantification of immunostaining intensity of nestin (*B*) and pS6RP (*C*) at the time points indicated following 2 Gy of γIR (SHH + N-myc and SHH + Akt-driven tumors). PVN in human medulloblastomas are very similar to those seen in mice. (*D*) Triple immunofluorescent merged images (pS6RP [green]/CD31 [red]/DAPI [blue], CD31 [red]]/nestin [green]/DAPI [blue], nestin [green]/pS6RP [red]/DAPI [blue], and nestin [green]/notch receptor [red]/DAPI [blue]) of human medulloblastoma samples showing existence of stem cell niches around blood vessels similar to mouse tumors (*n* = 2 frozen and 13 paraffin sections, total 15). Bars: *A*, 20 and 100 μm; *D*, 20 μm. Dunnett's Multiple Comparison Test of ANOVA was used. (\*\*) $P < 0.01$; (no asterisk) not significant.

induced elevation of p53 was PTEN-dependent. It also suggests that one reason that PTEN deficiency prevents radiation-induced cell cycle arrest may be due to the inability of such cells to elevate p53 levels. We then investigated to what degree the lack of p53 could mimic the loss of PTEN in the radiation response of the various cell types in these tumors.

Next, we created a medulloblastoma model in a p53-deficient background by overexpressing SHH + Akt and SHH + N-myc (*n* = 5 for 2-Gy γIR 6 h; *n* = 5 for control). All three cell types seen in the p53 wild-type tumors were found in these p53-deficient medulloblastomas, indicating that the p53 function is not required for the creation or maintenance of PVN, EN, and TB. Furthermore, the proliferation rate of the three cell types matched that of p53 wild-type tumors. The baseline levels of pS6RP and nestin were much higher in the p53-null tumors compared with those with wild-type p53

(data not shown). In these tumors, 2 Gy γIR induced elevation of pS6RP, nestin, and pAkt, indicating that p53 was not required for these radiation-induced effects. Following irradiation, almost all tumor cells were highly positive for pS6RP, nestin, and pAkt (data not shown).

*Radiation-induced cell cycle arrest and apoptosis are p53-dependent*

Although the cell types seen in p53 wild-type tumors were also present in the p53-null counterparts, the response of these cells to radiation was not always the same. The EN regions were unaffected by irradiation in both the p53-null and wild-type p53 tumors. This was consistent with the lack of p53 protein induction in the EN cells of wild-type p53 tumors and their lack of proliferation. However, unlike wild-type p53 tumors, the proliferating bulk of the p53-null tumors showed little
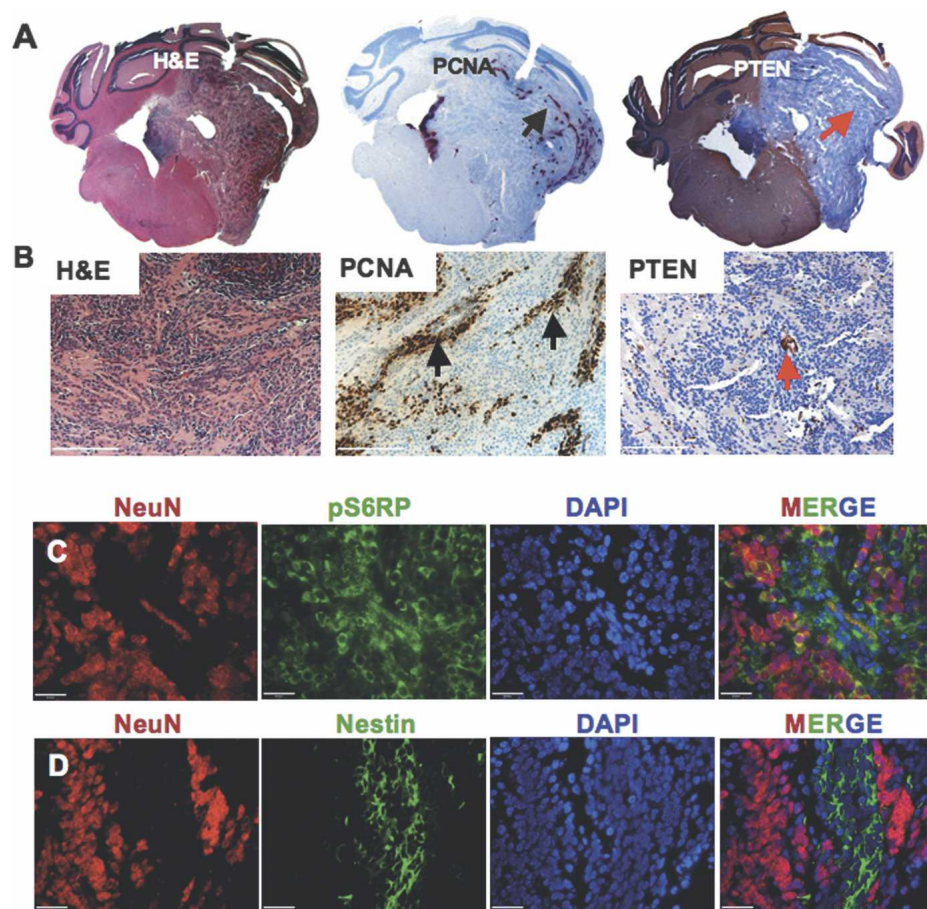
**Figure 5.** PTEN loss in combination with SHH overexpression leads to formation of medulloblastomas with EN in mice. Whole mount (*A*) and higher magnification (*B*) of H&E, PCNA, and PTEN immunoreactivity as indicated (black arrow represents proliferating cells of PVN and red arrow shows endothelial cells, the only PTEN-positive cells in the tumor). (*C*) Triple immunofluorescent staining of NeuN (red), pS6RP (green), and DAPI (blue) in the PVN. (*D*) Triple immunofluorescent staining of NeuN (red), nestin (green), and DAPI (blue). Bars: *B*, 100 μm; *C,D*, 20 μm.

radiation-induced cell death ($n$ = 5- to 6-h-post-2-Gy γIR) (Fig. 6B–D). Furthermore, the cells of the PVN that in p53 wild-type tumors elevated p53 levels and arrested at 6 h, showed no radiation-induced arrest in the p53-null background. This indicates that both the radiation-induced cell cycle arrest in the PVN and cell death in the TB of medulloblastomas were p53-dependent (Fig. 6B,C,E,F).

*Inhibition of the Akt pathway prior to irradiation decreases survival of the PVN*

We investigated whether inhibition of Akt signaling prior to irradiation decreases cell survival in the PVN of medulloblastoma. The basal levels of pAkt in SHH + N-myc tumors are nearly undetectable; thus, we used the SHH + Akt-induced tumor model. As these tumors show detectable basal levels of pAkt, it is possible to evaluate the effects of treatment by comparing any decreases in pAkt levels to vehicle-treated controls. First, we examined the effect of the small molecule in-

hibitor of Akt signaling, perifosine, on the pAkt levels in the SHH + Akt tumors. Perifosine treatment resulted in increased apoptosis and regional necrosis, but had no significant effect on the proliferation status of these tumors ($n$ = 3) (data not shown). To determine whether Akt inhibition prior to irradiation sensitizes the cells of the PVN to radiation-induced apoptosis, we pretreated tumor-bearing mice with perifosine for 3 d before irradiating with 2 Gy ($n$ = 3). Perifosine pretreatment completely abrogated radiation-induced phosphorylation of Akt and led to increased apoptosis in the PVN (Fig. 7A–C). This increased apoptosis was not due to a decrease in vasculature, as no changes in vascular density were observed. These results support the hypothesis that radiation-induced Akt phosphorylation in the PVN is responsible for the radioresistance of these cells, and that this effect can be reduced by pretreatment with perifosine.

**Discussion**

In this study, we describe the radiation response of a tumor model that has a well-defined stem cell niche.

Hambardzumyan et al.
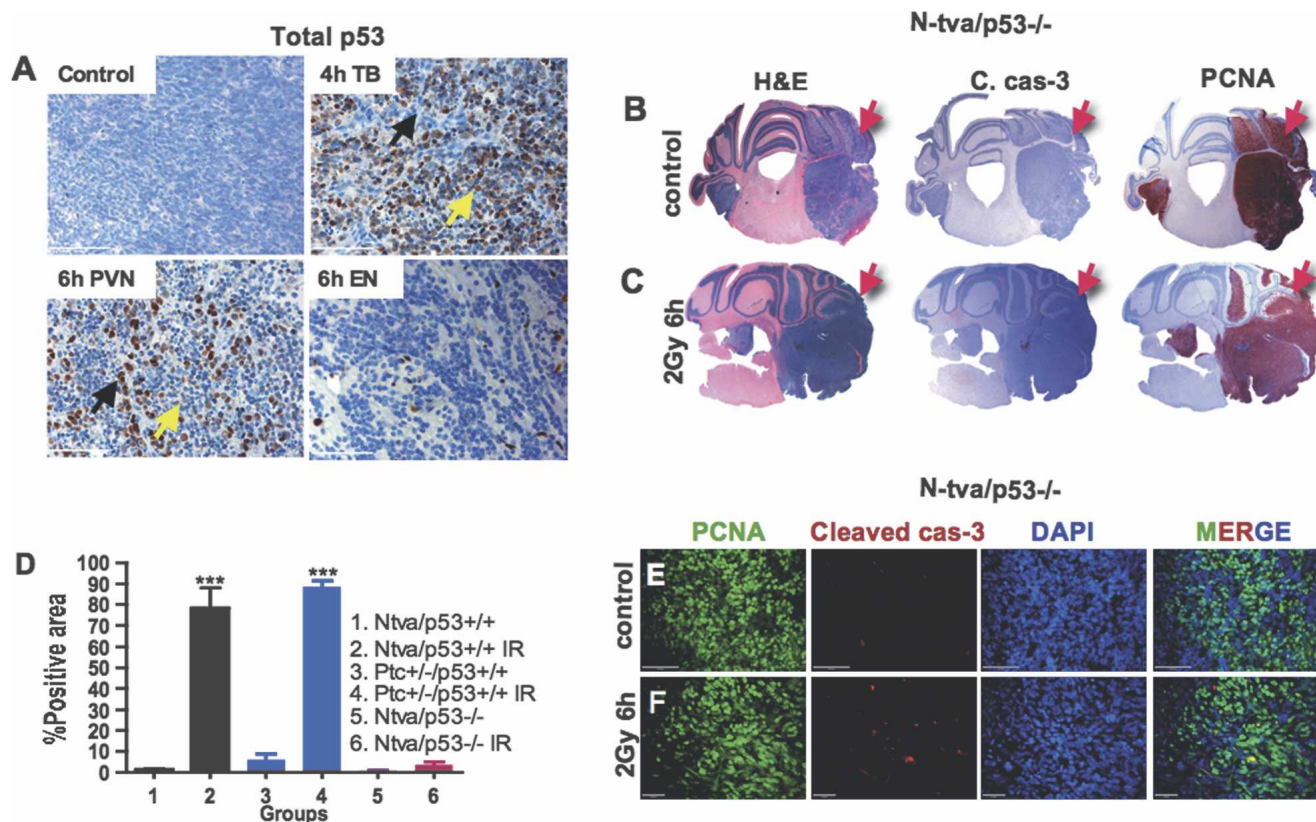


**Figure 6.** Radiation-induced cell death and cell cycle arrest are p53-dependent. (*A*) At 4 h, p53 is immunoreactive in the dying cells outside of the PVN; at 6 h, the cells of the PVN express p53 while the cells outside of the PVN have lost p53 expression (black arrow represents apoptotic cells, and yellow arrow represents arresting cells). Regions of EN do not elevate p53 expression following radiation (SHH + N-myc). Whole mounts of H&E, PCNA, and cleaved caspase-3 of control (*B*) and 6-h-post-γIR (*C*) tumors in N-tva/p53$^{-/-}$ background (SHH + Akt) (red arrows point to the tumor regions). (*D*) Quantification of cleaved caspase-3 staining in medulloblastomas untreated and treated with 2 Gy of γIR in different backgrounds with different combinations ($n = 4$ for groups 1 and 2; $n = 6$ for groups 3 and 4, which contain spontaneous medulloblastomas in *Ptc*$^{+/-}$ background and medulloblastomas in *Ptc*$^{+/-}$ background irradiated at P1; $n = 5$ for groups 5 and 6). Triple immunofluorescent images of PCNA (green), cleaved caspase-3 (red), and DAPI (blue) of untreated (*E*) and 6-h-post-γIR (*F*) tumors in Ntva/p53$^{-/-}$ background showing very little elevation of cleaved caspase-3. Bars: *A*, 50 µm; *E*, 20 µm; *F*, 100 µm. Two-sided *t*-test was used for *D*. (***) $P < 0.001$.

Our results illustrate the critical importance of using models that genetically and histologically mimic the human tumors in their natural environment in order to fully understand the biology of therapeutic response. If the model used to understand this biology does not recapitulate the various cell types in their native setting, the subtle but critical cell-type-specific responses may not be detected.

Our data support the previous reports of a cancer stem cell niche adjacent to the blood vessels in human medulloblastoma, as well as in a mouse model of this disease. We show that a single dose of radiation induces apoptosis in the main tumor population and cell cycle arrest in the stem cell compartment in a p53-dependent manner. We show for the first time that p53 has different effects within the same tumor, as it is necessary for radiation-induced cell death in the TB and cell cycle arrest in the PVN. The perivascular stem cells arrest at 6 h post-irradiation and re-enter the cell cycle at 72 h. Cells in PVN are all nestin-positive, and a subset of those cells

are also positive for GFAP and Olig2. A third cell population was identified in regions of EN that is nonproliferating, differentiated toward the neural lineage, and radiation-resistant. Both cell types that are radioresistant activate the PI3K/Akt/mTOR pathway; this effect is more pronounced in the PVN.

We confirm the importance of the PI3K/Akt/mTOR pathway in our SHH-driven medulloblastomas by generating a novel medulloblastoma model induced by SHH and PTEN loss that histologically resembles human medulloblastomas with EN. This tumor had high levels of Akt in the TB, resulting in neuronal post-mitotic differentiation as characterized by high NeuN levels. In the PVN, there was a high expression of nestin, pAkt, and PCNA. In addition, there was no radiation-induced cell death in the TB or cell cycle arrest in the PVN. These data demonstrate the role of PTEN in driving cell cycle arrest in the PVN and in driving differentiation in the TB. PTEN and Akt regulate both the radiation response of the PVN and the differentiation of the TB of SHH-
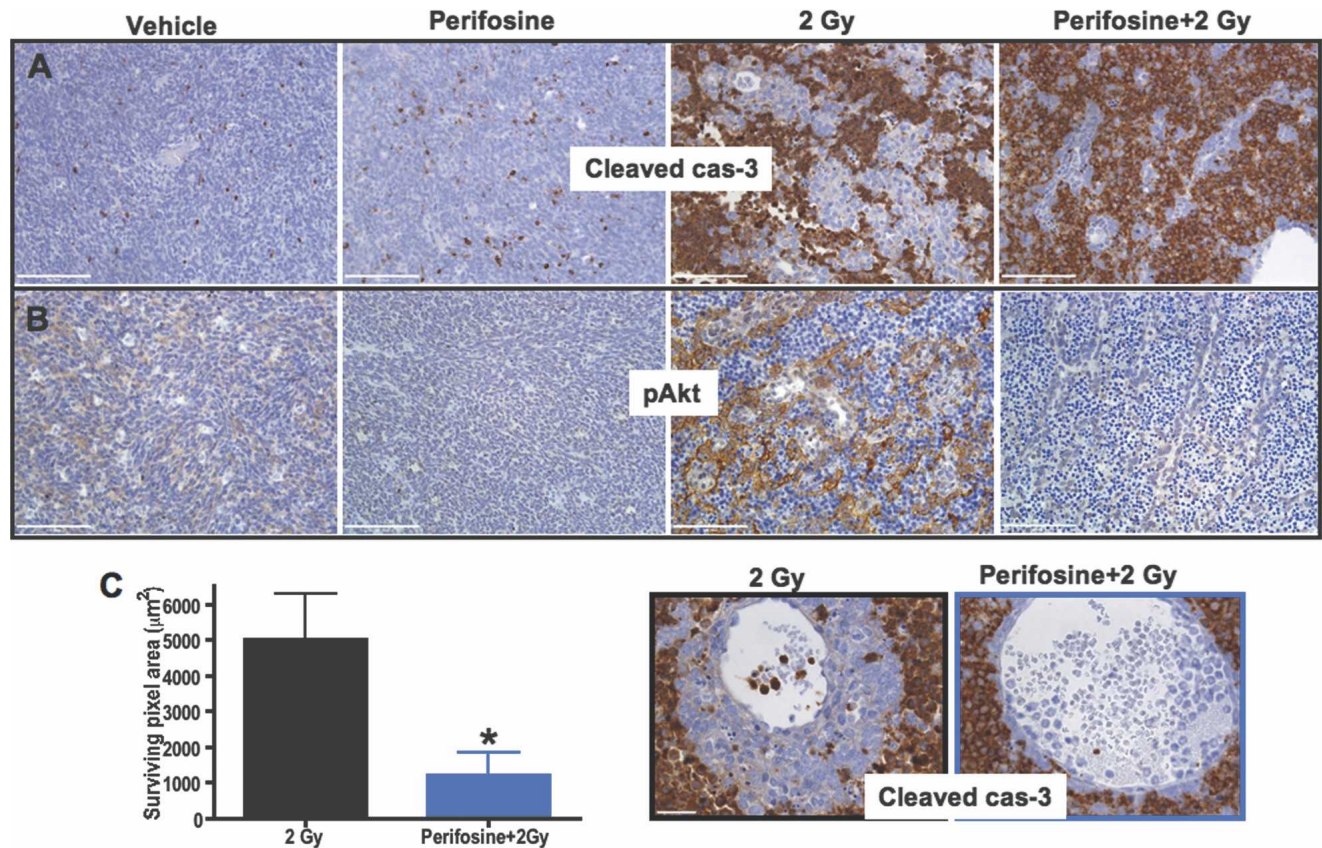
**Figure 7.** Perifosine inhibits Akt phosphorylation and sensitizes the PVN to radiation-induced cell death in SHH + Akt tumors. Perifosine was administered to tumor-bearing mice i.p. at 30 mgper kilogram daily for 3 d ($n = 3$). A control group was treated with saline ($n = 3$). At 12 h after the last dose, 2 Gy TBI was administered (Perifosine + 2 Gy, $n = 3$). Representative immunohistochemistry for cleaved cas-3 (*A*) and pAkt S473 (*B*). (*C*) Quantification of the surviving PVN area; representative photomicrographs of cleaved caspase-3 staining in 2 Gy and Perifosine + 2 Gy treatment groups are on the *left*. Fifteen 20× pictures were taken, the surviving areas were quantified, and averages were plotted. Bars: *A*,*B*, 100 µm,; *C*, 50 µm. Two-sided *t*-test was used in *C*. (*) $P < 0.05$.

driven medulloblastomas. Furthermore, our data suggests that Akt inhibition presents a rational clinical treatment paradigm that may increase the efficacy of clinically relevant doses of radiation.

## Materials and methods

### Cell culture and transfection

Df-1 cells were purchased from American Type Culture Collection (ATCC). Cells were grown at 39°C according to ATCC instructions. Transfections with RCAS-SHH, RCAS-N-myc-T50A, RCAS-AKT-Myr Δ11–60 and RCAS-Cre were performed using a FuGene 6 transfection kit (Roche, #11814443001) according to the manufacturer's instructions. Transfection efficacies were checked by Western blots and PCR.

### Generation of tumors using RCAS/TVA

Mice were injected within 48 h of birth with 1 µL of a 1:1 mixture of DF-1 cells producing RCAS-SHH in combination with RCAS-N-myc-T50A or RCAS-AKT-Myr Δ11–60 over the cerebellum of Ntv-a wild-type p53 and Ntv-a p53-null background mice, and RCAS-SHH and RCAS-Cre were injected into

Ntv-a/LPTEN mice. Mice were monitored carefully for symptoms of tumor development (hydrocephalus, lethargy, or head tilt).

### Radiation treatment

Total-body irradiation (TBI) was delivered with a ^{137}Cs irradiator (Shepherd Mark-I, model 68, SN 643) at a dose rate of 2.12 Gy per minute. Mice were sacrificed at different post-radiation time points.

*Drug administration.* Perifosine was obtained from Keryx Biopharmaceuticals; it is a novel Akt inhibitor. It belongs to a class of lipid-related compounds called alkylphospholipids. Tumor-bearing mice received i.p. 30 mg/kg perifosine daily for 3 d. For combined treatment with radiation, 12 h after the last dose of perifosine, mice were irradiated by 2 Gy TBI, and 6 h later mice from all groups were sacrificed.

### Generation of tumors in PTC^{+/−} background

In order to increase tumor incidence in PTC^{+/−} background, we used 3 Gy TBI at P1. Mice developed tumors at age 2–6 mo with 80%–85% tumor incidence.

Hambardzumyan et al.

## TUNEL assay

The TUNEL assay was performed on 5-μm sections by using a terminal transferase recombinant kit (Roche, #3333566) in accordance with the manufacturer's protocol.

## Immunofluorescent staining

Tumor-bearing animals were sacrificed and perfused under deep anesthesia (0.1 mg/g ketamine and 0.02 mg/g xylazine) by intracardiac infusion of 0.1 M phosphate buffer followed by perfusion with 10% formalin. Following perfusion, the brains were removed, post-fixed in 10% formalin for 72 h, paraffin-embedded, and cut into 5-μm sections. The sections were deparaffinized in Histo-Clear (Richard-Allan Scientific, #6901) and passed through graded alcohols. The next step was antigen retrieval with citric acid (Vector Laboratories #H-3300) in a boiling-water bath for 15 min. After two washes in PBS and permeabilization in 0.2% Triton in 0.1 M PBS for 45 min, sections were incubated in 0.1 M PBS containing 2% BSA, 5% NDS, and 0.1% Triton for 1 h at room temperature. For all mouse antibodies, MOM kit (Vector Laboratories, #BML-2202) was applied. For single staining, sections were incubated with the following antibodies overnight at 4°C in PBS plus 1% BSA: primary anti-cleaved caspase-3 diluted 1:100 (Cell Signaling, #9661), anti-GFAP (DAKO, #Z0334), anti-pS6RP diluted 1:100 mouse and 1:50 human (Cell Signaling, #2211), anti-CD34 diluted 1:50 (Abcam, #ab8158), anti-PCNA diluted 1:100 (Calbiochem, #NA03, 0.8), anti-Olig 2 diluted 1:250 (Chemicon, #AB9610), anti-nestin 401 diluted 1:100 (BD Pharmingen, #556309), anti-NeuN diluted 1:100 (Chemicon, #MAB377), anti-notch diluted 1:100 (Abcam, #ab3294), anti-PTEN diluted 1:100 (Cell Signaling, #9559), anti-AktT308 diluted 1:50 (Cell Signaling, #9266), anti-Akt S473 (Cell Signaling, #9277), and anti-CD31 diluted 1:50 (Dako, #NO823). For immunofluorescence staining after primary antibody, the secondary antibodies conjugated to different Alexa-Fluor dyes (488, 555, 647) at a dilution of 1:500 in PBS were applied. For nuclear counterstaining, DAPI was used.

## Immunohistochemistry

For immunohistochemical detection, an automated staining processor was used (Discovery, Ventana Medical Systems, Inc.). The protocols were established at the Molecular Cytology Core Facility at Memorial Sloan-Kettering Cancer Center (MSKCC).

## Human tissue specimens

Two human medulloblastoma samples were obtained from the MSKCC tissue bank with the approval of the institutional review board. The samples were flash-frozen in liquid nitrogen immediately following removal and stored at –80°C. Then, fresh-frozen 5-μm sections were fixed with 4% paraformaldehyde and immunofluorescence and immunohistochemistry were performed as described above. Besides the fresh-frozen sections, we obtained 13 human medulloblastoma paraffin sections from the Department of Pathology at MSKCC. The patients were not treated with either radiation or chemotherapy.

## Quantification of histology

Immunofluorescent images were quantified using the Metamorph imaging system and program. From all of the groups, the brightest staining was taken to find the fixed exposure time, and the rest of the pictures were taken at the same exposure time.

Ten of the 20× images were taken per tumor, and the total gray value per pixel area was quantified. For quantification of immunohistochemistry, 10 of the 20× pictures were taken per tumor and the positive (brown) area was quantified using Metamorph and plotted as percentage of total area. For quantification of the surviving PVN area, 15 of the 20× pictures were analyzed. The lumen of the vessels and few apoptotic cells in PVN were subtracted from the total surviving area.

## Statistical analysis

Graphs were made using GraphPad Prism 4 (GraphPad Software) and were analyzed using ANOVA and two-sided $t$-tests. For Figure 3, C and D, we used Dunnett's Multiple Comparison Test of ANOVA, which compares all columns versus the control column. For Figure 6D, we used Excel and a two-sided $t$-test that compares a 2-Gy 6-h column versus the control column. (*) $P < 0.05$; (**) $P < 0.01$; (***) $P < 0.001$; (no asterisk) not significant.

## Acknowledgments

## References

Ahmed, N.N., Grimes, H.L., Bellacosa, A., Chan, T.O., and Tsichlis, P.N. 1997. Transduction of interleukin-2 antiapoptotic and proliferative signals via Akt protein kinase. *Proc. Natl. Acad. Sci.* **94:** 3627–3632.

Alvarez-Buylla, A., Seri, B., and Doetsch, F. 2002. Identification of neural stem cells in the adult vertebrate brain. *Brain Res. Bull.* **57:** 751–758.

Bao, S., Wu, Q., McLendon, R.E., Hao, Y., Shi, Q., Hjelmeland, A.B., Dewhirst, M.W., Bigner, D.D., and Rich, J.N. 2006. Glioma stem cells promote radioresistance by preferential activation of the DNA damage response. *Nature* **444:** 756–760.

Browd, S.R., Kenney, A.M., Gottfried, O.N., Yoon, J.W., Walterhouse, D., Pedone, C.A., and Fults, D.W. 2006. N-myc can substitute for insulin-like growth factor signaling in a mouse model of sonic hedgehog-induced medulloblastoma. *Cancer Res.* **66:** 2666–2672.

Calabrese, C., Poppleton, H., Kocak, M., Hogg, T.L., Fuller, C., Hamner, B., Oh, E.Y., Gaber, M.W., Finklestein, D., Allen, M., et al. 2007. A perivascular niche for brain tumor stem cells. *Cancer Cell* **11:** 69–82.

Cogen, P.H. and McDonald, J.D. 1996. Tumor suppressor genes and medulloblastoma. *J. Neurooncol.* **29:** 103–112.

Corcoran, R.B. and Scott, M.P. 2001. A mouse model for medulloblastoma and basal cell nevus syndrome. *J. Neurooncol.* **53:** 307–318.

Dahmane, N. and Ruiz i Altaba, A. 1999. Sonic hedgehog regulates the growth and patterning of the cerebellum. *Development* **126:** 3089–3100.

Dee, S., Haas-Kogan, D.A., and Israel, M.A. 1995. Inactivation of p53 is associated with decreased levels of radiation-induced apoptosis in medulloblastoma cell lines. *Cell Death Differ.* **2:** 267–275.

Deutsch, M., Thomas, P.R., Krischer, J., Boyett, J.M., Albright, L., Aronin, P., Langston, J., Allen, J.C., Packer, R.J., Linggood, R., et al. 1996. Results of a prospective randomized trial comparing standard dose neuraxis irradiation (3,600 cGy/20) with reduced neuraxis irradiation (2,340 cGy/13) in patients with low-stage medulloblastoma. A combined Children's Cancer Group–Pediatric Oncology Group study. *Pediatr. Neurosurg.* **24:** 167–176.

Eberhart, C.G., Chaudhry, A., Daniel, R.W., Khaki, L., Shah, K.V., and Gravitt, P.E. 2005. Increased p53 immunopositivity in anaplastic medulloblastoma and supratentorial PNET is not caused by JC virus. *BMC Cancer* **5:** 19. doi: 10.1186/1471-2407-5-19.

Fisher, G.H., Orsulic, S., Holland, E., Hively, W.P., Li, Y., Lewis, B.C., Williams, B.O., and Varmus, H.E. 1999. Development of a flexible and specific gene delivery system for production of murine tumor models. *Oncogene* **18:** 5253–5260.

Goodrich, L.V., Milenkovic, L., Higgins, K.M., and Scott, M.P. 1997. Altered neural cell fates and medulloblastoma in mouse patched mutants. *Science* **277:** 1109–1113.

Hahn, H., Christiansen, J., Wicking, C., Zaphiropoulos, P.G., Chidambaram, A., Gerrard, B., Vorechovsky, I., Bale, A.E., Toftgard, R., Dean, M., et al. 1996. A mammalian patched homolog is expressed in target tissues of sonic hedgehog and maps to a region associated with developmental abnormalities. *J. Biol. Chem.* **271:** 12125–12128.

Hambardzumyan, D., Squatrito, M., and Holland, E.C. 2006. Radiation resistance and stem-like cells in brain tumors. *Cancer Cell* **10:** 454–456.

Hammerschmidt, M., Brook, A., and McMahon, A.P. 1997. The world according to hedgehog. *Trends Genet.* **13:** 14–21.

Hemmati, H.D., Nakano, I., Lazareff, J.A., Masterman-Smith, M., Geschwind, D.H., Bronner-Fraser, M., and Kornblum, H.I. 2003. Cancerous stem cells can arise from pediatric brain tumors. *Proc. Natl. Acad. Sci.* **100:** 15178–15183.

Hershatter, B.W., Halperin, E.C., and Cox, E.B. 1986. Medulloblastoma: The Duke University Medical Center experience. *Int. J. Radiat. Oncol. Biol. Phys.* **12:** 1771–1777.

Hitoshi, S., Alexson, T., Tropepe, V., Donoviel, D., Elia, A.J., Nye, J.S., Conlon, R.A., Mak, T.W., Bernstein, A., and van der Kooy, D. 2002. Notch pathway molecules are essential for the maintenance, but not the generation, of mammalian neural stem cells. *Genes* & *Dev.* **16:** 846–858.

Holland, E.C. and Varmus, H.E. 1998. Basic fibroblast growth factor induces cell migration and proliferation after glia-specific gene transfer in mice. *Proc. Natl. Acad. Sci.* **95:** 1218–1223.

Ignatova, T.N., Kukekov, V.G., Laywell, E.D., Suslov, O.N., Vrionis, F.D., and Steindler, D.A. 2002. Human cortical glial tumors contain neural stem-like cells expressing astroglial and neuronal markers in vitro. *Glia* **39:** 193–206.

Kennedy, S.G., Wagner, A.J., Conzen, S.D., Jordan, J., Bellacosa, A., Tsichlis, P.N., and Hay, N. 1997. The PI 3-kinase/Akt signaling pathway delivers an anti-apoptotic signal. *Genes* & *Dev.* **11:** 701–713.

Kulik, G., Klippel, A., and Weber, M.J. 1997. Antiapoptotic signalling by the insulin-like growth factor I receptor, phosphatidylinositol 3-kinase, and Akt. *Mol. Cell. Biol.* **17:** 1595–1606.

Landberg, T.G., Lindgren, M.L., Cavallin-Stahl, E.K., Svahn-Tapper, G.O., Sundbarg, G., Garwicz, S., Lagergren, J.A., Gunnesson, V.L., Brun, A.E., and Cronqvist, S.E. 1980. Improvements in the radiotherapy of medulloblastoma, 1946–1975. *Cancer* **45:** 670–678.

Lee, Y. and McKinnon, P.J. 2002. DNA ligase IV suppresses medulloblastoma formation. *Cancer Res.* **62:** 6395–6399.

Lee, Y., Miller, H.L., Jensen, P., Hernan, R., Connelly, M., Wetmore, C., Zindy, F., Roussel, M.F., Curran, T., Gilbertson, R.J., et al. 2003. A molecular fingerprint for medulloblastoma. *Cancer Res.* **63:** 5428–5437.

Marino, S., Vooijs, M., van Der Gulden, H., Jonkers, J., and Berns, A. 2000. Induction of medulloblastomas in p53-null mutant mice by somatic inactivation of Rb in the external granular layer cells of the cerebellum. *Genes* & *Dev.* **14:** 994–1004.

Packer, R.J. 1990. Chemotherapy for medulloblastoma/primitive neuroectodermal tumors of the posterior fossa. *Ann. Neurol.* **28:** 823–828.

Pazzaglia, S., Mancuso, M., Atkinson, M.J., Tanori, M., Rebessi, S., Majo, V.D., Covelli, V., Hahn, H., and Saran, A. 2002. High incidence of medulloblastoma following X-ray-irradiation of newborn Ptc1 heterozygous mice. *Oncogene* **21:** 7580–7584.

Pazzaglia, S., Tanori, M., Mancuso, M., Rebessi, S., Leonardi, S., Di Majo, V., Covelli, V., Atkinson, M.J., Hahn, H., and Saran, A. 2006. Linking DNA damage to medulloblastoma tumorigenesis in patched heterozygous knockout mice. *Oncogene* **25:** 1165–1173.

Pietsch, T., Waha, A., Koch, A., Kraus, J., Albrecht, S., Tonn, J., Sorensen, N., Berthold, F., Henk, B., Schmandt, N., et al. 1997. Medulloblastomas of the desmoplastic variant carry mutations of the human homologue of *Drosophila* patched. *Cancer Res.* **57:** 2085–2088.

Pomeroy, S.L., Tamayo, P., Gaasenbeek, M., Sturla, L.M., Angelo, M., McLaughlin, M.E., Kim, J.Y., Goumnerova, L.C., Black, P.M., Lau, C., et al. 2002. Prediction of central nervous system embryonal tumour outcome based on gene expression. *Nature* **415:** 436–442.

Portwine, C., Chilton-MacNeill, S., Brown, C., Sexsmith, E., McLaughlin, J., and Malkin, D. 2001. Absence of germline and somatic p53 alterations in children with sporadic brain tumors. *J. Neurooncol.* **52:** 227–235.

Raffel, C., Jenkins, R.B., Frederick, L., Hebrink, D., Alderete, B., Fults, D.W., and James, C.D. 1997. Sporadic medulloblastomas contain PTCH mutations. *Cancer Res.* **57:** 842–845.

Rao, G., Pedone, C.A., Coffin, C.M., Holland, E.C., and Fults, D.W. 2003. c-Myc enhances sonic hedgehog-induced medulloblastoma formation from nestin-expressing neural progenitors in mice. *Neoplasia* **5:** 198–204.

Rao, G., Pedone, C.A., Valle, L.D., Reiss, K., Holland, E.C., and Fults, D.W. 2004. Sonic hedgehog and insulin-like growth factor signaling synergize to induce medulloblastoma formation from nestin-expressing neural progenitors in mice. *Oncogene* **23:** 6156–6162.

Schmitt, C.A., Fridman, J.S., Yang, M., Baranov, E., Hoffman, R.M., and Lowe, S.W. 2002. Dissecting p53 tumor suppressor functions in vivo. *Cancer Cell* **1:** 289–298.

Singh, S.K., Clarke, I.D., Terasaki, M., Bonn, V.E., Hawkins, C., Squire, J., and Dirks, P.B. 2003. Identification of a cancer stem cell in human brain tumors. *Cancer Res.* **63:** 5821–5828.

Songyang, Z., Baltimore, D., Cantley, L.C., Kaplan, D.R., and Franke, T.F. 1997. Interleukin 3-dependent survival by the Akt protein kinase. *Proc. Natl. Acad. Sci.* **94:** 11345–11350.

Strojnik, T., Rosland, G.V., Sakariassen, P.O., Kavalar, R., and Lah, T. 2007. Neural stem cell markers, nestin and musashi proteins, in the progression of human glioma: Correlation of nestin with prognosis of patient survival. *Surg. Neurol.* **68:** 133–143.

Tong, W.M., Ohgaki, H., Huang, H., Granier, C., Kleihues, P., and Wang, Z.Q. 2003. Null mutation of DNA strand break-binding molecule poly(ADP-ribose) polymerase causes me-

dulloblastomas in p53$^{-/-}$ mice. *Am. J. Pathol.* **162:** 343–352.

Wallace, V.A. 1999. Purkinje-cell-derived Sonic hedgehog regulates granule neuron precursor cell proliferation in the developing mouse cerebellum. *Curr. Biol.* **9:** 445–448.

Wechsler-Reya, R.J. and Scott, M.P. 1999. Control of neuronal precursor proliferation in the cerebellum by Sonic Hedgehog. *Neuron* **22:** 103–114.

Weiner, H.L., Bakst, R., Hurlbert, M.S., Ruggiero, J., Ahn, E., Lee, W.S., Stephen, D., Zagzag, D., Joyner, A.L., and Turnbull, D.H. 2002. Induction of medulloblastomas in mice by sonic hedgehog, independent of Gli1. *Cancer Res.* **62:** 6385–6389.

Wetmore, C., Eberhart, D.E., and Curran, T. 2000. The normal patched allele is expressed in medulloblastomas from mice with heterozygous germ-line mutation of patched. *Cancer Res.* **60:** 2239–2246.

Wetmore, C., Eberhart, D.E., and Curran, T. 2001. Loss of p53 but not ARF accelerates medulloblastoma in mice heterozygous for patched. *Cancer Res.* **61:** 513–516.

Wolter, M., Reifenberger, J., Sommer, C., Ruzicka, T., and Reifenberger, G. 1997. Mutations in the human homologue of the *Drosophila* segment polarity gene patched (PTCH) in sporadic basal cell carcinomas of the skin and primitive neuroectodermal tumors of the central nervous system. *Cancer Res.* **57:** 2581–2585.

Woodburn, R.T., Azzarelli, B., Montebello, J.F., and Goss, I.E. 2001. Intense p53 staining is a valuable prognostic indicator for poor prognosis in medulloblastoma/central nervous system primitive neuroectodermal tumors. *J. Neurooncol.* **52:** 57–62.

Yan, X., Fraser, M., Qiu, Q., and Tsang, B.K. 2006. Over-expression of PTEN sensitizes human ovarian cancer cells to cisplatin-induced apoptosis in a p53-dependent manner. *Gynecol. Oncol.* **102:** 348–355.

Yuan, X., Curtin, J., Xiong, Y., Liu, G., Waschsmann-Hogiu, S., Farkas, D.L., Black, K.L., and Yu, J.S. 2004. Isolation of cancer stem cells from adult glioblastoma multiforme. *Oncogene* **23:** 9392–9400.

Zindy, F., Nilsson, L.M., Nguyen, L., Meunier, C., Smeyne, R.J., Rehg, J.E., Eberhart, C., Sherr, C.J., and Roussel, M.F. 2003. Hemangiosarcomas, medulloblastomas, and other tumors in Ink4c/p53-null mice. *Cancer Res.* **63:** 5420–5427.

# PI3K pathway regulates survival of cancer stem cells residing in the perivascular niche following radiation in medulloblastoma in vivo

Dolores Hambardzumyan, Oren J. Becher, Marc K. Rosenblum, et al.

| | |
|---|---|
| **Supplemental Material** | http://genesdev.cshlp.org/content/suppl/2008/02/15/22.4.436.DC1 |
| **References** | This article cites 51 articles, 22 of which can be accessed free at: http://genesdev.cshlp.org/content/22/4/436.full.html#ref-list-1 |
| **License** | |
| **Email Alerting Service** | Receive free email alerts when new articles cite this article - sign up in the box at the top right corner of the article or **click here.** |